Biotite surface chemistry as a function of aqueous fluid composition

Andrew W. Bray [a,b,*], Liane G. Benning [a], Steeve Bonneville [c], Eric H. Oelkers [b]

[a] Cohen Geochemistry, School of Earth and Environment, University of Leeds, Leeds LS2 9JT, United Kingdom
[b] Géochimie et Biogéochimie Expérimentale, GET CNRS, UMR 5563, 14 av. Edouard Belin, 31400 Toulouse, France
[c] Biogéochimie et Modélisation du Système Terre, Département des Sciences de la Terre et de l'Environnement, Université Libre de Bruxelles, 50 av. F.D. Roosevelt, 1050 Brussels, Belgium

Abstract

The chemical composition and charge of the biotite near-surface, in contact with NaCl bearing aqueous solutions at 25 °C from pH 1 to 12, have been derived via zeta potential measurements and potentiometric titrations performed for 20 and 60 min in batch reactors. Zeta potential measurements yielded an isoelectric point of pH 3.0 ($\pm$0.2) and batch potentiometric titrations yielded a pH of immersion of 9.66 (S.D. 0.24). From batch potentiometric titrations we determined both the proton consumption and the metal release from the biotite surface as a function of pH. Potassium removal from the near-surface of biotite is only slightly dependent on pH with a minimum of $\sim$6 atoms nm^{-2} removed at the immersion pH, corresponding to an average depletion depth of $\sim$1.5 nm. In contrast, the release of Mg, Al and Fe is strongly pH-dependent as those metals are preferentially removed from the biotite surface at pH less than 9 (Mg) and 4 (Al, Fe). The average depletion depth of Mg, Al, and Fe increases with decreasing pH, reaching on average $\sim$2 nm at pH $\sim$1. The removal of K, Mg, Al, and Fe is not charge conservative, resulting in a relative negative charge in the biotite near-surface. Taken together, our results indicate that the composition of the biotite surface varies dramatically as a function of pH. At basic conditions, the biotite near-surface is K depleted and likely hydrogen enriched. At near-neutral conditions, the biotite near-surface is comprised of only the Si and Al tetrahedral, and the Fe(II) octahedral framework, following the removal of both alkali metals and Mg. Finally, at acidic conditions, the biotite near-surface is comprised exclusively of a remnant Si, O and H framework. The results of these experiments give an indication of the composition and charge of the biotite surface in the natural environment, following contact with water, for example in the vadose zone, and can help us understand weathering reactions in these systems.

1. INTRODUCTION

Mineral surface composition and charge are often linked to mineral reactivity and adsorption properties (e.g. Pokrovsky et al., 1999; Sverjensky, 2004). Among the most significant minerals in the subsurface, in terms of controlling the chemical composition and evolution of surface waters, are the phyllosilicates (including clays). This is due to their large surface areas and high ion-exchange capacity (Sposito, 1984; Davis and Kent, 1990; Drever, 1997; Bowser and Jones, 2002). Several recent studies reported that due to metal exchange reactions, the composition of the near-surface of multi-oxide minerals depends strongly on the composition of its surrounding aqueous phase (e.g. Pokrovsky and Schott, 2000; Chaïrat et al., 2007; Oelkers et al., 2009). In an attempt to extend these concepts to phyllosilicates, we have performed a series of batch potentiometric titration experiments and electrokinetic measurements on biotite surfaces as a function of aqueous solution pH from 1 to 12. The purpose of this paper is to report the results of these experiments aimed towards the improved understanding of how

---

* Corresponding author at: Cohen Geochemistry, School of Earth and Environment, University of Leeds, Leeds LS2 9JT, United Kingdom. Tel.: +44 01133435220.
E-mail addresses: a.bray@see.leeds.ac.uk (A.W. Bray), L.G.Benning@leeds.ac.uk (L.G. Benning).

the surface compositions of phyllosilicate minerals are influenced by the aqueous phase composition.

Mineral surface chemistry has often been linked to dissolution rates (Morel and Hering, 1993). Early studies attempted to correlate mineral surface charge to the concentration of surface-sites, determined via potentiometric titrations as a function of pH (e.g. Furrer and Stumm, 1986; Brady and Walther, 1990; Pokrovsky and Schott, 2004). This approach has subsequently been questioned by observations that in addition to proton absorption and desorption a large number of reactions influence proton consumption during potentiometric titrations (e.g. Oelkers et al., 2009). Furthermore, dissolution rates of a wide range of minerals can depend on the activity of aqueous metals present in solution (e.g. Gautier et al., 1994; Oelkers et al., 1994; Devidal et al., 1997; Gislason and Oelkers, 2003; Wolff-Boenisch et al., 2004; Carroll and Knauss, 2005; Saldi et al., 2007). A further motivation of this study is therefore to characterise the reactions controlling the surface chemistry of a reference phyllosilicate, biotite, to improve our understanding of the overall dissolution mechanism of this widespread family of minerals.

A further motivation for a quantitative understanding of the surface properties and dissolution behaviour of phyllosilicates is due to their significance as a nutrient source in the terrestrial environment. A number of studies have reported on the crucial role of micro-organisms in weathering primary minerals and acquiring key nutrients (e.g. Leyval and Berthelin, 1991; Drever and Stillings, 1997; Wallander and Wickman, 1999; Adeyemi and Gadd, 2005; Buss et al., 2007; Gadd, 2007; Lian et al., 2008; Smits et al. 2012). Several studies focussed on biotite weathering and metal acquisition by bacteria (e.g. Balland et al., 2010) and fungi (e.g. Balogh-Brunstad et al., 2008; Bonneville et al., 2009, 2011). Remarkably, for fungi, the weathering process is a combination of mechanical forcing of the biotite near-surface and several chemical alteration pathways. These studies also demonstrated that the near-surface properties of biotite are crucial in controlling the initiation of weathering processes. Yet, how the chemistry of the biotite near-surface influences both nutrient availability and the mechanism of micro-organism nutrient acquisition is still unknown.

In this study, we have assessed the degree to which the biotite near-surface chemistry is influenced by the composition of its surrounding aqueous phase. We have done this through a series of batch potentiometric experiments at 25 °C and between pH 1 and 12, which were also complimented through electrokinetic measurements. Titration results were interpreted to (i) evaluate the main contributing reaction types occurring at the biotite surface and (ii) determine how the composition of the biotite surface varies as a function of pH.

2. EXPERIMENTAL METHODS

2.1. Mineral sample

The biotite used in this study originated from the Grasåsen feldspar quarry, Moen, Arendal, Aust-Agder, Norway (sourced from Agder Naturmuseum, Kristiansand). A large piece ($\sim$600 g) was broken into chunks and all visible inclusions were removed. For the chemical characterisation, a polished block of the biotite was imaged using a field emission gun scanning electron microscope (FEG-SEM, FEI Quanta 650 equipped with an Oxford X-Max silicon drift detector, SDD and operated at 20 kV). The biotite, along with inclusions and areas of alteration, was imaged and characterised using backscattered electron emission (BSE) and energy-dispersive X-ray spectroscopy (EDX). The bulk chemical composition of the biotite was characterised by electron microprobe analysis (EMPA, Jeol JXA-8230 running with a tungsten source at 15 kV and 15 nA) using the average of 15 point measurements ($\sum$oxide weight > 99%) and $O_{10}(OH)_2$ formula units. The electron microprobe analysis of the Grasåsen biotite yielded the following chemical composition ($K_{0.913}$ $Na_{0.011}$ $Ca_{0.0002}$) ($Mg_{1.436}$ $Mn_{0.004}$ $Fe^{(II)}_{1.098}$ $Cr^{(II)}_{0.0004}$)($Al_{1.312}$ $Ti^{(IV)}_{0.184}$ $Si^{(IV)}_{2.832}$)$(OH)_2(O)_{10}$.

The remaining biotite was crushed using a ball mill, jaw crusher, and agate disk mill, removing visible inclusions throughout. The <53 μm size fraction was separated and further crushed for use in the batch potentiometric and electrokinetic measurements. Crushed biotite grains were imaged using FEG-SEM and grains were observed to be between sub-micron and 10 μm in size (Fig. S-1). The specific surface area (s) of this crushed biotite fraction was measured via an 11 point krypton adsorption isotherm that was run from 0.046 to 0.30 p/p_o (equilibrium pressure/saturation pressure) at 77 K, on a Quantachrome AUTO-SORB-1. Samples were degassed with Kr at 120 °C for 23 h before analysis and the surface area was calculated using the BET method (Brunauer et al., 1938) based on an assumed cross section of absorbed Kr of 0.205 nm^2. The specific surface area of the Grasåsen biotite was calculated to be 13.43 m^2 g^{-1}. The average metal site density at the biotite surface was estimated to be 10 nm^{-2} using VESTA (Momma and Izumi, 2011) for visualising the biotite structure as presented by Brigatti et al. (2000). The crushed biotite was also analysed by X-ray fluorescence (XRF, Innov-x X-5000) at 10 kV and X-ray diffraction (XRD, Bruker D8) with a scan range from 5° to 75° 2θ and a step size of 0.009° 2θ, to give an indication of any impurities within the crushed fraction. Reitveld refinement of XRD patterns by Topas software version 4.2 (copyright 1999–2009 Bruker AXS) indicated the presence of 3.7 wt.% ($\pm$0.5%) calcite, supported by 1.36 wt.% calcium ($\approx$3.4% calcite) as measured by XRF. Apart from the presence of calcium, XRF analysis provided a composition consistent with the biotite stoichiometry determined by EMPA.

2.2. Batch potentiometric titrations

A total of 65 time limited, biotite-bearing batch experiments were performed at 25 °C which, when taken together, represent a potentiometric titration series, as previously described by Pokrovsky et al. (1999) and Oelkers et al. (2009). In brief, 20 g/L of biotite was equilibrated while stirred in a polypropylene reactor with a NaCl electrolyte of known ionic strength (I) for at least 12 h under a N$_2$ atmosphere (5.0 grade). Batch reactions were performed by mixing $\sim$7 ml

aliquots of this pre-equilibrated biotite suspension with a known quantity of analytical grade HCl or NaOH in 15 ml polypropylene vials. Experiments were conducted under a N_2 atmosphere, for either 20 or 60 min and were shaken constantly at 140 rpm, with additional manual shaking every 10 min. At the end of each titration experiment, the pH in each vial was measured using a Metrohm 713 pH Meter, calibrated with certified reference buffer solutions of pH 4.005, 6.866, and 9.183 (CertiPUR, Merck) at 25 °C.

After pH measurement, the fluid from each batch experiment was filtered through 0.2 μm cellulose acetate Sartorius Minisart filters (and stored at 4 °C analysis. The concentrations of Na, Mg, Al, K, Ca, Ti, Cr, Mn, and Fe in the filtered reactor fluids were determined by inductively coupled plasma mass spectrometry (ICP-MS, Thermo Agilent 1700C; maximum analytical uncertainty ± 5%) while aqueous silicon, Si, was determined using the colorimetric molybdate blue method (Bran & Luebbe AutoAnalyzer 3, maximum analytical uncertainty ± 3.5%).

A control titration series was obtained through otherwise identical experiments using biotite-free fluids, i.e., from the pre-equilibrated biotite suspension filtered through a 0.2 μm cellulose acetate Nalgene filter unit. The control titration series was performed to determine a baseline for data interpretation.

Full details of all biotite-bearing and biotite-free batch titration experiments can be found in Tables A-1 and A-2, respectively, in Appendix A. Details include mineral suspension concentration, fluid ionic strength, experiment time, suspension volume, and titrant concentration at the start of the experiment ($t = 0$); and, pH and fluid composition at the end of each titration.

2.3. Electrokinetic measurements

The electrophoretic mobility of the biotite powder was measured at 25 °C using a Zetaphoremetre IV, model Z3000 microelectrophoremeter with a dielectric constant of 80 ± 1 V. For each measurement, biotite powder was added to individually prepared aqueous NaCl or HCl solutions ($I = 10^{-1}$ to 10^{-3} M) with pH from 1 to 12 and measured within 5 min by electrophoresis. As in the batch titrations, the pH range for electrophoretic measurements was attained through the addition of analytical grade HCl or NaOH. The pH of each fluid sample was measured externally during electrophoresis. Measured electrophoretic mobilities were converted to ζ potentials using the Smoluchowski equation (Hunter, 1989) and are presented in Table A-3 in Appendix A, along with the details of solution compositions used for electrophoretic measurement.

3. THEORETICAL BACKGROUND

This study builds from our current understanding of the mineral–fluid interface (c.f. Parks, 1965, 1967, 1990; Davis and Kent, 1990; Sposito 1998; Pokrovsky and Schott, 2000; Oelkers et al., 2009; Brown and Calas, 2012). A large number of terms are necessary to describe these interfaces, and their definitions can be ambiguous, thus, we briefly review some of these here.

The zero point of charge (pH_{ZPC}) is the pH value where, regardless of source, the net charge at the surface of a material is zero.

There are three primary methods for determining the pH_{ZPC} of minerals. (1) The isoelectric point (pH_{IEP}), as determined by electrokinetic measurements, indicates the pH at which there is no net charge at the hydrodynamic shear-plane of a particle in solution; and therefore, the point at which there is no movement of particles in an electric field (note that ions can adsorb to the mineral surface and hence contribute to the charge at the hydrodynamic shear-plane and, therefore, to pH_{IEP}). (2) Acid–base potentiometric titrations of a mineral yield the point of zero net proton charge (pH_{ZNPC}), the point at which the concentrations of H^+ and OH^- ions consumed by a surface are equal, therefore giving the surface a net neutral charge. This is synonymous with the pH of an aqueous solution in equilibrium with a mineral, when no titrant has been added, also referred to in this study as the immersion pH (pH_{imm}). (3) The common intersection point of acid–base titration curves at two or more ionic strengths yields the point of zero salt effect (pH_{PSZE}).

When there is no internal net charge on the mineral and in the absence of ions for adsorption, other than H^+ and OH^-, $pH_{IEP} = pH_{ZNPC} = pH_{PZSE} = pH_{ZPC}$ (Sposito, 2004). However, in a large number of cases $pH_{IEP} \neq pH_{PZSE}$ (c.f. Sverjensky, 2004) and in such cases the pH_{IEP} determined at low ionic strengths (e.g. 0.001–0.01 M) may be more representative of pH_{ZPC} (Sverjensky, 1994). Furthermore, to accurately model the mineral surface, both the surface composition and the electrochemical state must be considered. Both these parameters can be determined via potentiometric titrations by quantifying proton consumption at both the mineral surface and in all other proton-consuming reactions. These in turn can all be determined from accurate pH measurements in combination with aqueous analysis of the dissolved species present during the titration.

In this study, the total amount of protons consumed, normalised to mineral surface area, ($[H_{tot}^+]$, atoms nm^{-2}) during timed batch titration experiment was derived from the difference between the calculated proton concentration in each reactor at the start of each titration ($[H^+]_{t=0}$, mol kg^{-1}) and the concentration of protons determined from the measured pH of the aqueous suspension, after its interaction with biotite powder ($[H^+]_{t=t}$, mol kg^{-1}). The value of $[H^+]_{t=0}$ was calculated using:

$$[H^+]_{t=0} = \frac{((m_a M_a) + (m_e M_e))}{(M_a + M_e)} \qquad (1)$$

where m_a and m_e (mol kg^{-1}) correspond to the concentration of protons in the added titrant and the mineral–electrolyte suspension, respectively, while M_a and M_e (kg) designate the masses of these fluids. Proton concentration at the end of each experiment $[H^+]_{t=t}$ was calculated from the measured pH, such that

$$[H^+]_{t=t} = \left(\frac{10^{-pH}}{\gamma_{H^+}} \right) - \left(\frac{10^{-(-\log(K_{H_2O}) - pH)}}{\gamma_{OH^-}} \right) \qquad (2)$$

where γ_i designates the activity coefficient of the ith aqueous species, calculated using the Davies equation (Davies, 1962), and K_{H_2O} stands for the water ionisation constant (10^{-14}; IUPAC, 2006). Combining Eqs. (1) and (2) leads to $[H_{tot}^+]$ which can be represented as (adapted from Oelkers et al., 2009):

$$[H_{tot}^+] = ([H^+]_t = 0 - [H^+]_{t=t})\left(\frac{N}{Ms10^{18}}\right) \qquad (3)$$

where N designates Avogadro's number (6.02×10^{23}), M (kg) the mass of mineral powder, and s (m^2 kg^{-1}) the biotite powder specific surface area. The quantity of protons consumed due to the presence of biotite ($[H_s^+]$, atoms nm^{-2}) was calculated by subtracting from $[H_{tot}^+]$ the protons consumed in an equivalent biotite-free titration at each corresponding pH ($[H_0^+]$, atoms nm^{-2})

$$[H_s^+] = [H_{tot}^+] - [H_0^+] \qquad (4)$$

where $[H_0^+]$, for a given pH, was interpolated from a regression of the biotite-free titration curve (after an immersion period of 12 h, see Section 2.2).

During each batch titration, protons were consumed or produced by reactions occurring either in the aqueous solution ($[H_{sol}^+]$) or through incorporation into/onto mineral surfaces ($[H_{surf}^+]$), such that:

$$[H_s^+] = [H_{sol}^+] + [H_{surf}^+] \qquad (5)$$

During the titration, three proton related, aqueous solution-based reactions occur (Eq. (6)): (i) biotite dissolution, $[H_{dis}^+]$, (ii) calcite dissolution $[H_{carb}^+]$ and (iii) hydrolysis of aqueous cations, $[H_{hy}^+]$, such that $[H_{sol}^+]$ can be written as:

$$[H_{sol}^+] = [H_{dis}^+] + [H_{carb}^+] + [H_{hy}^+] \qquad (6)$$

Similarly, two reactions can incorporate protons onto or into the mineral surface (Eq. (7)): (i) metal exchange reactions, $[H_{ex}^+]$, and (ii) proton adsorption, $[H_{ad}^+]$ and therefore $[H_{surf}^+]$ can be written as:

$$[H_{surf}^+] = [H_{ex}^+] + [H_{ad}^+] \qquad (7)$$

Combining Eqs. (5)–(7) allow formulation of the following expression for the total number of protons consumed via aqueous solution-based and mineral surface reactions (Eq. (8)):

$$[H_s^+] = [H_{dis}^+] + [H_{carb}^+] + [H_{hy}^+] + [H_{ex}^+] + [H_{ad}^+] \qquad (8)$$

Details on these five proton-related reactions are presented below with representative worked examples outlined in Appendix B.

3.1. Biotite dissolution reactions

In this study, biotite dissolution was assumed to be stoichiometric and consistent with Si release, thus the dissolution reaction can be represented as:

$$\sum_i (n_i z_i)H^+ + \sum_i (M_i)_{n_i}SiO_{2+} \sum_i \left(\frac{n_i z_i}{2}\right)$$
$$= \sum_i (n_i M_i^{z_i}) + SiO_2(aq) + \sum_i \left(\frac{n_i z_i}{2}\right)H_2O \qquad (9)$$

where n_i refers to the stoichiometric coefficient of metal M_i in the biotite formula, normalised to one Si, and z_i the charge of the M_ith free ion in aqueous solution. Through the dissolution of one biotite molecule $\sum_i (n_i z_i)$ protons are consumed. Therefore, the number of protons consumed by dissolution, $[H_{dis}^+]$, is proportional to the number of Si atoms released to the fluid, so that:

$$[H_{dis}^+] = \sum_i (n_i z_i)[Si_s] \qquad (10)$$

where $[Si_s]$ (atoms nm^{-2}) is the surface area normalised number of Si atoms released into aqueous solution during the titration.

3.2. Calcite dissolution reactions

The quantitative XRD analyses of our starting material revealed the presence of 3.7 wt.% calcite. The release of 1 mol of Ca from calcite dissolution is accompanied by the release of 1 mol of CO_3^{2-}. The released CO_3^{2-} is present in solution as either CO_3^{2-}, HCO_3^- or H_2CO_3, depending on pH, with the latter two species consuming 1 and 2 protons respectively. In a CO_2 free system, the total carbonate concentration [carbonate$_s$] (atoms nm^{-2}) is equal to the calcium concentration released from calcite dissolution [Ca$_{carb,s}$] (atoms nm^{-2}). This can be calculated from:

$$[\text{carbonate}_s] = [Ca_{carb,s}] = [Ca_s] - n_{Ca}[Si_s] \qquad (11)$$

where, $[Ca_s]$ represents the surface area normalised total calcium concentration, $n_{Ca}[Si_s]$ represents the contribution of Ca released from biotite dissolution. The concentrations of the carbonate species are calculated using the PHREEQC 3 computer code (Parkhurst and Appelo, 2013) and proton consumption by calcite dissolution $[H_{carb}^+]$ based on:

$$[H_{carb}^+] = ([H_2CO_3] \times 2) + [HCO_3^-] \qquad (12)$$

where, $[H_2CO_3]$ and $[HCO_3^-]$ represent the concentrations of carbonic acid and bicarbonate in aqueous solution, respectively.

3.3. Aqueous hydrolysis

The hydrolysis of aqueous metals in aqueous solution can be written as:

$$M_i^{z+} + n_H H_2O = M_iOH_{n_H}^{(z_i - n_H)} + n_H H^+ \qquad (13)$$

where n_H is the stoichiometric coefficient. In addition, above pH 9, silicic acid dissociates following:

$$SiO_2 + 2H_2O = H_3SiO_4^- + H^+ \qquad (14)$$

and therefore the net proton change induced by hydrolysis, normalised to mineral surface area, can be written:

$$\left[H_{hy}^{+}\right] = \left(\frac{N(M_a + M_e)}{Ms10^{18}}\right)\left(-\sum\left(n_H m_{M_iOH_{n_H}^{(z_in_H)+}}\right) - m_{H_3SiO_4^-}\right) \tag{15}$$

$\left[H_{hy}^{+}\right]$ (atoms nm^{-2}) is calculated by combining Eq. (13) with speciation calculations performed using the PHREEQC 3 computer code (Parkhurst and Appelo, 2013).

3.4. Metal–proton exchange reactions

In addition to stoichiometric dissolution of biotite, a fraction of total dissolved metals can be attributed to metal–proton exchange reactions. The amount of dissolved metals solubilised via exchange reactions can be calculated as:

$$[M_{i,ex}] = [M_{i,s}] - n_i[Si_s] \tag{16}$$

where $[M_{i,ex}]$ (atoms nm^{-2}) represents the number of M_i atoms exchanged from biotite during each batch titration experiment and $[M_{i,s}]$ (atoms nm^{-2}) represents the number of M_i atoms released to aqueous solution, normalised to the measured biotite surface area, while $n_i[Si_s]$ represents the concentration of the ith element ascribed to stoichiometric dissolution. Metal exchange from a surface can coincide with proton consumption:

$$> M_i + n_{M_i,ex}H^+ = M_i^{z_i+} + > H_{n_{M_i,ex}}^{(n_{M_i,ex} - z_i)+} \tag{17}$$
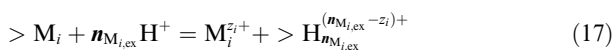
where $>M_i$ and $> H_{n_{M_i,ex}}^{(n_{M_i,ex} - z_i)+}$ stand for a mineral surface site filled with a metal or proton respectively, and $n_{M_i,ex}$ denotes the number of protons consumed by the mineral surface for the exchange of one M_i atom. Therefore, the total number of protons that could be consumed by all exchange reactions ($[H_{ex}^{+}]$), if charge is conserved, is equal to:

$$\left[H_{ex}^{+}\right] = \sum_i (n_{M_i,ex})[M_{i,ex}] \tag{18}$$

Reaction (17) allows for the replacement of M_i with more or less protons than is necessary for charge balance. A number of previous studies have concluded that charge balance is not always retained during metal–proton exchange reactions. For example, Oelkers et al. (2009) reported that 3.8 protons are consumed by the removal of each Mg from forsterite, 3.1 to 3.3 protons are consumed by the removal of each Mg or Ca from diopside or enstatite, and 1.4 protons are consumed by the removal of Ca from wollastonite. Yet, such a non-conservation of charge is not necessarily true for all metal exchange reactions, and for example, albite dissolution has been interpreted to proceed via charge conservation with respect to Al exchange (Oelkers et al., 2009). This aspect is discussed in more detail below.

3.5. Surface adsorption

The last aspect of proton consumption that needs to be considered is the adsorption and desorption of protons from hydroxyl surface sites, following the generic reactions:

$$> M_iOH^0 + H^+ => M_iOH_2^+ \tag{19}$$

and

$$> M_iOH^0 => M_iO^- + H^+ \tag{20}$$

The proportion of these reactions to the total proton consumption ($[H_{ad}^{+}]$) can be calculated using Eq. (8), after first calculating the contributions from dissolution, hydrolysis and metal–proton exchange processes. Eqs. (1)–(20) are used below to interpret proton consumption by reactions occurring at the biotite surface during batch titration reactions. Results are discussed in terms of atoms nm^{-2}, allowing ready comparison to literature data on mineral surface reactive site density.

4. RESULTS

Results show that the concentration of protons consumed by biotite, during the titration series, increases with decreasing pH. The minimum proton consumption occurs at pH $\sim$10, consistent with the immersion pH (pH$_{imm}$). The total amount of metals released from dissolution and metal–proton exchange reactions increases with decreasing pH. Electrokinetic measurements performed over 3 orders of magnitude of ionic strength yielded an isoelectric point at pH $\sim$3. These results will be presented in detail below.

4.1. Batch potentiometric titrations

4.1.1. Proton consumption

Total proton consumption during the 65 biotite-bearing batch experiments performed in this study is shown in Fig. 1. It can be seen that proton consumption during the 20 min titration series are identical, within uncertainty, to the corresponding proton consumption during the 60 min titrations (Fig. 1A). The pH values of the biotite suspension after the immersion period (pH$_{imm}$, also depicted in Fig. 1A) yield an average of 9.66 (S.D. 0.24; $n = 7$). The batch titration series from biotite-bearing and biotite-free experiments yield two distinct functions and are presented on a plot of log[H$^+$]$_{t=0}$ against pH in Fig. 1B. The results shown in Fig. 1B appear to be independent of the fluid ionic strength (e.g., NaCl concentration). In all cases, the pH of the biotite-free series is lower than the corresponding pH in the biotite-bearing reactors, indicating that fluid–biotite interaction consumed protons during the titrations. At a given pH, the difference between these two curves corresponds to $[H_s^{+}]$, as defined in Eq. (4), and calculated using the cubic regression of the biotite-free titration results shown in Fig. 1B.

The number of protons consumed by all reactions occurring in the presence of the biotite, $[H_s^{+}]$, dramatically changes with pH (Fig. 2). At pH $\sim$1, this value exceeds 100 atoms nm^{-2}, and decreases to zero at the immersion pH (pH$_{imm}$). The $[H_{sol}^{+}]$ and $[H_{surf}^{+}]$ values shown in Fig. 2 were calculated using Eqs. (6) and (7) and correspond to the number of protons consumed via dissolution and metal hydrolysis, and metal–proton exchange and adsorption, respectively. It should be noted that $[H_{sol}^{+}]$ is similar to $[H_s^{+}]$ above pH $\sim$3, meaning that the contribution of $[H_{surf}^{+}]$ is approximately 0 in this region.
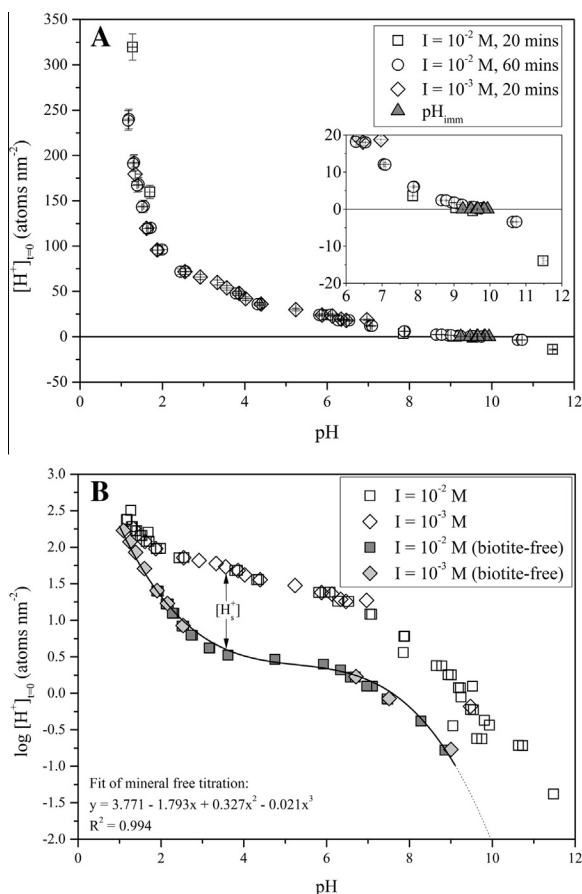
Fig. 1. Concentration of protons in the batch titration reactors at time zero ($[H^+]_{t=0}$, atoms nm^{-2}) against final measured pH ($t = 20$ or 60 min) at 25 °C and I of 0.01 or 0.001 M. Note the difference in y-axis of the plots with (A) linear, and (B) logarithmic. Values of 0 $[H^+]_{t=0}$ in (A) indicate the immersion pH (pH$_{imm}$), shown more clearly in the inset graph. Note also the two distinct curves in (B), the lower curve represents data from biotite free titrations ($[H_0^+]$) and is fitted with a cubic regression resulting in the formula given. The difference between the two curves in (B) is the value of $[H_s^+]$ as calculated in Eq. (4). The uncertainty of each data point yields error bars within the symbol ($\pm 4.5\%$ for $[H^+]_{t=0}$ and ± 0.002 pH).

4.1.2. Dissolution dependent and independent metal release

The surface area and biotite-stoichiometry normalised concentration of metal M_i removed from the biotite near-surface during the timed batch titrations ($[M_{i,s,b}]$, Fig. 3), decreases with increasing pH. From 16 to 6 atoms nm^{-2} of potassium is removed from the biotite surface from pH 1 to 12 respectively (Fig. 3A). Approximately 6 atoms nm^{-2} of K are released immediately at the start of the titration as indicated by the value of K released at pH$_{imm}$. The release of magnesium, iron, aluminium, and silicon (Fig. 3A and B), systematically increases with decreasing pH, with silicon being released least from the biotite near-surface when normalised to the solid phase composition. Consistent with the theoretical formalism described above (Section 3.1, Eqs. (9) and (10)), Si release is attributed solely to biotite dissolution, while the release of the other metals is attributed to a combination of dissolution and metal–proton exchange reactions. The concentrations of several minor and trace
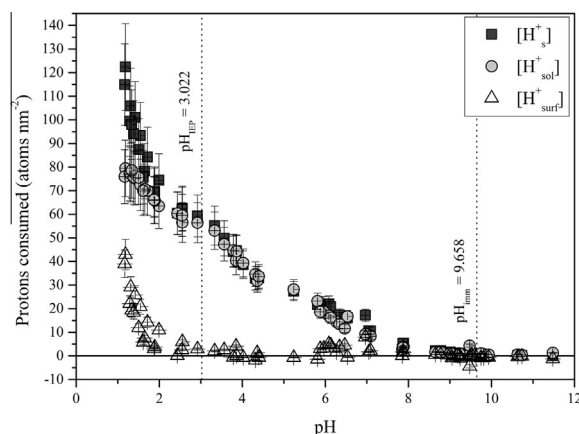

Fig. 2. Number of protons consumed by $[H_s^+]$, $[H_{sol}^+]$ and $[H_{surf}^+]$ (atoms nm^{-2}) plotted as a function of pH. Error bars represent a 15% [H$^+$] and 0.002 pH unit uncertainties. The dashed lines correspond to the pH$_{IEP}$ and pH$_{imm}$ for the Grasåsen biotite, as determined in this study.

metals released from the biotite near-surface during batch titrations are listed in Table A-1 along with the concentration of the background electrolyte (NaCl, see Na) which is also presented in the inset of Fig. 3B. It is worth noting that the high concentrations of Ca found in the aqueous solutions is consistent with the dissolution of approximately 3.2 ± 0.5 wt.% calcite, comparable to the 3.4–3.7 wt.% calcite present in the biotite powder, as determined by XRF and XRD.

The release of metals from the biotite near-surface by exchange reactions ($[M_{i,ex}]$) is also highly pH dependent (Fig. 4). Using Fig. 4 we can highlight a number of important observations. First, by definition, a metal exchange, $[M_{i,ex}]$, value of 0 atoms nm^{-2} indicates stoichiometric dissolution, while $[M_{i,ex}] > 1$ indicates preferential release and $[M_{i,ex}] < 1$ indicates preferential retention (Fig. 4). Results show that at the pH of immersion (pH$_{imm}$, 9.66) $\sim$6 K atoms nm^{-2} are released. As the stoichiometric release of K from dissolution (based on the average Si concentration at pH$_{imm}$) is 0.16 atoms nm^{-2}, at the immersion pH, $\sim$97% of the K in solution is a result of metal–proton exchange. With decreasing pH, $[K_{ex}]$ increases systematically, attaining a maximum value of approximately 10 atoms nm^{-2} at pH 1, where dissolution contributes only $\sim$38% of dissolved K in the fluid. In contrast, $[Mg_{ex}]$, $[Fe_{ex}]$, and $[Al_{ex}]$ are close to 0 atoms nm^{-2} at the pH$_{imm}$. With decreasing pH, $[Mg_{ex}]$, $[Fe_{ex}]$, and $[Al_{ex}]$ increase steadily with decreasing pH when pH is less than $\sim$9, $\sim$4 and $\sim$4, respectively, reaching between 6 to 10 atoms nm^{-2} at pH $\sim$1. Furthermore, $[Fe_{ex}]$ and $[Al_{ex}]$ are both negative at pH between 4 and 8, while $[Mg_{ex}]$ is negative at the most alkaline pH values ($>$10.5). This suggests that at these conditions, these metals are preferentially retained by the biotite surfaces.

4.2. Electrokinetic measurements

The ζ potential values of the ground biotite particles in aqueous solutions of ionic strength from 0.001 to 0.1 M

Fig. 4. Quantity of metals exchanged from the biotite surface, normalised to surface area, ($[M_{i,ex}]$, atoms nm^{-2}, Eq.) as a function of pH. The solid line where $[M_{i,ex}] = 0$ indicates stoichiometric biotite dissolution. Error bars represent an uncertainty of 15% in $[M_{i,ex}]$ and 0.002 pH units.
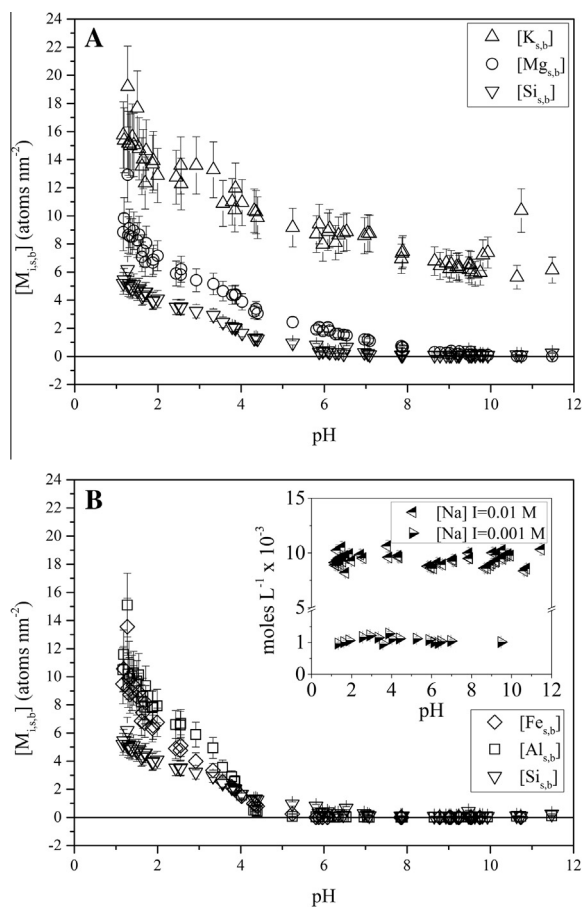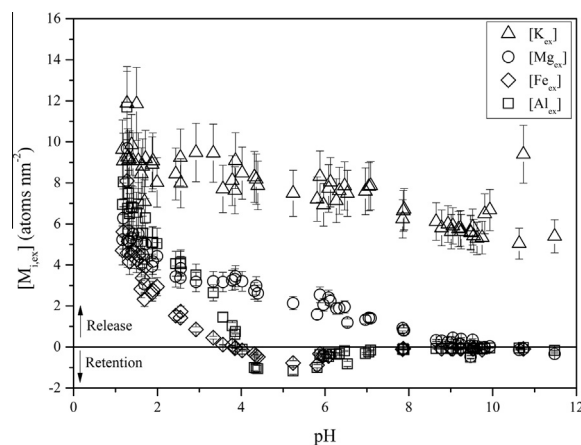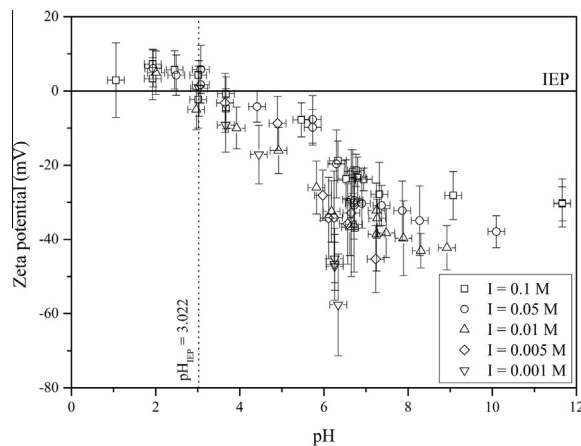

Fig. 3. Quantity of metals released from the biotite surface during batch titrations, normalised to mineral surface area present in the reactor and mineral stoichiometry, ($[M_{i,s,b}]$, atoms nm^{-2}) plotted as a function of pH for; (A) $[K_{s,b}]$, $[Mg_{s,b}]$ and $[Si_{s,b}]$, and (B) $[Fe_{sb}]$, $[Al_{s,b}]$ and $[Si_{s,b}]$. The concentration the background electrolyte (Na, corrected for NaOH addition, es L^{-1} × 10^{-3}) is plotted as a function of pH in the inset of B. Error bars represent uncertainty of 15% $[M_{i,s,b}]$, [Na] and 0.002 pH units.

Fig. 5. Zeta potential (mV) at five ionic strengths plotted against pH. The dashed line corresponds to the pH where zeta potential $= 0$, pH_{IEP}. Error bars represent 2 standard deviations of each zeta potential and 0.2 pH units.

NaCl converge at zero ζ potential (Fig. 5). The point of zero ζ potential is the isoelectric point (pH_{IEP}) and occurs at pH 3.02. The pH_{IEP} of biotite in this study is listed in Table 1 together with the values of pH_{IEP} of other comparable minerals from literature. The full list of electrophoretic mobilities measured, and corresponding ζ potentials can be found in Table A-3 in Appendix A.

5. DISCUSSION

5.1. Non-stoichiometric metal release and charge conservation

The degree to which metal exchange reactions are charge balanced by protons can be assessed with the aid of Fig. 6. For charge balance, the sum of equivalence of the released metals (concentration of exchanged metals multiplied by corresponding charge) should correspond to the number of protons consumed by surface reactions $[H_{surf}^+]$, indicated

by the $y = x$ line. Charge balance can occur either by H$^+$ incorporation into the structure $[H_{ex}^+]$ or H$^+$ adsorption onto the mineral surface, both of which are accounted for in $[H_{surf}^+]$. As can be seen in Fig. 6, the relationship between total equivalence and $[H_{surf}^+]$ is far from 1:1. As there is a proton consumption deficit, it appears that metals are removed from the biotite structure without significant charge conservation.

The non-conservation of charge due to metal release is supported by the pH_{IEP} value of 3.02 obtained for this biotite. This value is lower than the calculated pH_{ZPC} and pH_{ZNPC} (see Section 5.3 for details) and can be explained by the observed metal release. If metals are released without a compensating incorporation of protons, the surface becomes increasingly negative. The combination of a relatively negative near-surface and the tendency of the

Table 1
pH of various zero points of charge determined in this study unless otherwise stated.

Mineral	pH_{imm}	pH_{IEP}	pH_{zpc}
α-SiO$_2$	–	1.3[a], 2.0[b]	2.91[c], 2.3–3.8[d]
MgO	–	12.4[e]	12.24[c]
α-Fe$_2$O$_3$	–	5.4–6.9[e]	6[d]
^{IV}Al$_2$O$_3$	–	6.8[f]	8.5–9[d]
Muscovite	–	0.95[a]	6.6[c]
Phlogopite	–	–	8[e]
Biotite	–	0.41[a], 2.6[g]	6.5[h], 6–7[i]
Grasåsen Biotite (this study)	9.66	3.02	4.12[j], 7.50[k]

[a] Cases (1967).
[b] James and Healy (1972).
[c] Sverjensky (1994).
[d] Kosmulski (2009).
[e] Parks (1965).
[f] Parks (1967).
[g] Rath and Subramanian (1997).
[h] Alonso (2003, as cited by Filby et al., 2008).
[i] Alonso et al. (2009).
[j] Calculated from component single oxide pH_{IEP} values using Eq. (22).
[k] pH_{ZNPC} calculated correcting for H^+ consumed during immersion by dissolution and hydrolysis reactions, non stoichiometric K release, and carbonate equilibiria.
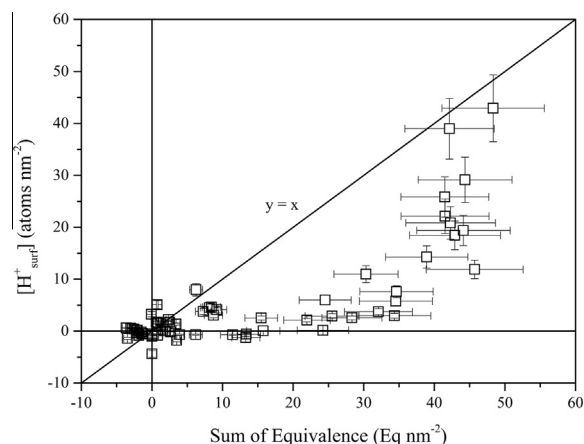

Fig. 6. Plot of $\left[H_{surf}^+\right]$ (atoms nm^{-2}) against the sum of equivalence for exchanged metals, $\Sigma([M_{i,ex}] \times z_{M_i})$, excluding K_{ex}. Error bars 15% uncertainty in the calculation of both $\left[H_{surf}^+\right]$ and the sum of equivalence.

surface to become Si–O rich, causes the isoelectric point (pH_{IEP}) to be at a lower pH than that which would be estimated from a sum of oxide mineral pH_{ZPC} and pH_{ZNPC} values.

At pH < pH_{IEP} (pH < ~3) $\left[H_{surf}^+\right]$ increases significantly (Fig. 2). This can be attributed to the consumption of protons by adsorption onto the biotite surface. Consistent with the non-conservation of charge of metal release, the remaining consumption of protons by surface reactions $\left[H_{surf}^+\right]$ corresponds to proton adsorption. In this pH region, where the surface of biotite is predominantly Si, the adsorption of H^+ forms partly detached silanol groups.
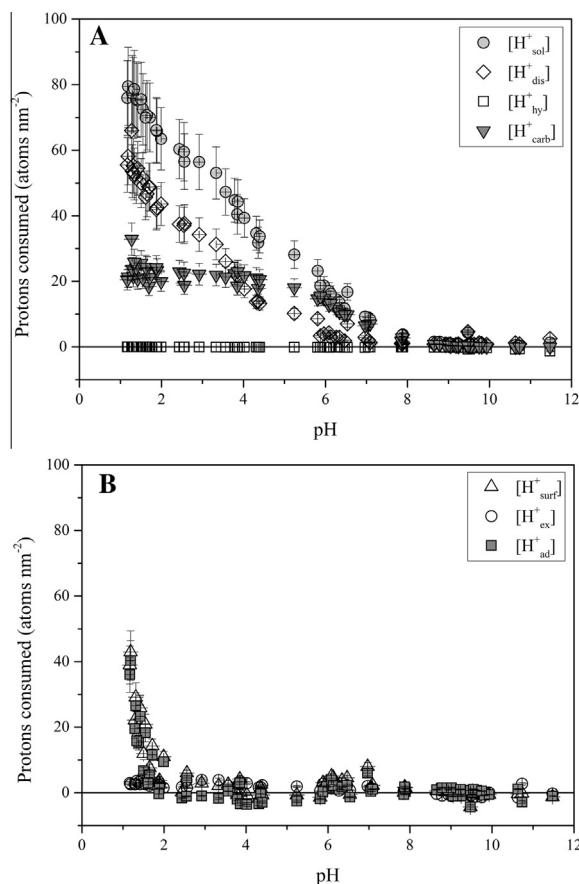

Fig. 7. Proton consumption as a function of pH for (A) $\left[H_{sol}^+\right]$ reactions and, (B) $\left[H_{surf}^+\right]$ reactions. $\left[H_{sol}^+\right]$ reactions in (A) include dissolution reactions ($\left[H_{dis}^+\right]$ and $\left[H_{carb}^+\right]$) and aqueous metal hydrolysis $\left[H_{hy}^+\right]$. $\left[H_{surf}^+\right]$ reactions in (B) include metal exchange reactions ($\left[H_{ex}^+\right]$) and proton adsorption ($\left[H_{ad}^+\right]$). Error bars represent 15% uncertainty in [H^+] and 0.002 pH unit uncertainty.

The relative contributions of proton consumption are presented in Fig. 7. Dissolution reactions, $\left[H_{dis}^+\right]$ and $\left[H_{carb}^+\right]$ dominate proton consumption (Fig. 7A). The contribution from metal hydrolysis $\left[H_{hy}^+\right]$ is negligible at all pH, because at low pH, metals in solution are present as single ions and at high pH, the aqueous concentration of dissolved metals is too low to contribute significantly. As mentioned above, $\left[H_{ex}^+\right]$ and $\left[H_{ad}^+\right]$ are relatively insignificant at pH > 3 (Fig. 7B).

5.2. Biotite surface composition as a function of pH

The results summarised above provide insight on how the surface chemistry of biotite varies as a function of the pH of the adjacent fluid. An understanding of the degree to which the biotite near-surface is altered by interaction with the adjacent fluid phase is aided by the calculation of the average bulk depletion depth of the major constituent metals (Dep_{M_i}).

$$Dep_{M_i} = \frac{[M_{i,ex}]}{\textbf{nb}_{M_i}\left(\frac{\rho_{biotite}}{m_{biotite}} \cdot \frac{N}{10^{21}}\right)} \quad (21)$$

The average bulk depth of metal M_i depletion (Dep_{M_i}) is calculated by dividing $[M_{i,ex}]$ by the average density of metal atoms M_i in the biotite structure (atoms nm^{-3}), where nb_{M_i} represents the stoichiometric coefficient of the M_ith metal in the bulk biotite, $\rho_{biotite}$ (g cm^{-3}) signifies the biotite density (3.09, average from webmineral.com) and $m_{biotite}$ (g mol^{-1}) the molecular mass of biotite (450.15 g mol^{-1}, for the Grasåsen biotite). Dep_{M_i} is calculated assuming that there is an abrupt change between the near-surface that is affected by the metal exchange reactions (i.e. a metal-free zone) and the bulk, non metal exchanged, mineral. The average depletion depth of each metal is illustrated as a function of pH in Fig. 8.

As can be seen in Fig. 8, potassium is calculated to be totally removed from biotite to a depth of ~1.5 nm at pH_{imm}. The Dep_K due to the titration alone can be calculated by subtracting the value of Dep_K at pH_{imm}. Charge balance constraints suggest that this K removal is accompanied by the incorporation of compensating positive ions into the biotite. This compensating positive charge can be partially attributed to the incorporation of H^+ into the interlayer sites, as demonstrated by the values of pH_{imm} ranging from pH 9.2 to 10 (Table A-1). However, a 1:1 charge compensation would require 10^{-3} protons, far exceeding the observed increase in pH from a theoretical pH 7 (computed due to the absence of CO_2) to pH_{imm}. This, therefore, leaves two possibilities, either (1) the charge is compensated by a different mono or divalent cation, or (2) K^+ release is not completely charge conservative. Taking the first option, it is possible that Na from the background electrolyte could substitute in the structure for K. If Na for K substitution was responsible for a complete charge compensation then it could be expected that Na concentrations would change substantially from the original concentration during the immersion period. The degree to which this happens can be assessed through Fig. 3B and Table A-1. As the concentration of Na does not significantly change with pH it is more feasible that the release of K^+ is non-charge conservative.

In contrast, Dep_{Mg} from the biotite surface increases continuously with decreasing pH. Similar to the behaviour of the magnesium in diopside and fosterite (Oelkers et al., 2009), magnesium in biotite is preferentially retained by the mineral at pH > 10, and increasingly depleted at pH < 8. Notably, the average magnesium depletion depth at neutral conditions ranges from 0.2 to 0.5 nm. As the concentration of Mg in the biotite structure is 5.9 atoms nm^{-3} (Eq. (21)), the depletion depth results (Fig. 8) suggest that 1 to 3 atoms nm^{-2} of Mg would have been removed from the biotite surface at the pH of most natural waters. This depletion corresponds to 20–50% Mg removal from the first unit cell of biotite.

The behaviour of Dep_{Al} and Dep_{Fe} exhibit similar variations with pH at the biotite surface (Fig. 8). Both metals are present in the mineral in close-to-stoichiometric quantities at pH greater than 8. Al and Fe are preferentially retained by the solid phase from pH 4 to 8 and removed to an increasing depth with decreasing pH when pH < 4. This preferential retention of Fe and Al by the solid phase at pH 4 to 8, and Mg above pH 10, may originate from either secondary phase precipitation or preferential retention by the biotite. The former possibility is supported by the calculated saturation state of the fluid phase during the titrations (Fig. 9). Between pH 4 and 11, aluminium and iron oxyhydroxides are both supersaturated in the fluid phase while some Mg-rich clays are supersaturated in the fluid phases of the titrations performed at pH > 9. Comparing the dissolved concentrations of Al and Fe at pH (4–8) to that found at the pH_{imm} indicates precipitation. It is therefore likely that Al and Fe oxy-hydroxides formed in these experiments on the biotite surfaces. These values of Dep_{M_i} are calculated assuming an isotropic biotite structure. Phyllosilicates are, however, highly anisotropic. The actual metal depletion depth (Dep_{M_i}) in biotite is likely to be highly heterogeneous due to the nature of the biotite surfaces (e.g., edges vs. basal surfaces). Turpault and Trotignon (1994) and Hodson (2006) have shown biotite edge surfaces are
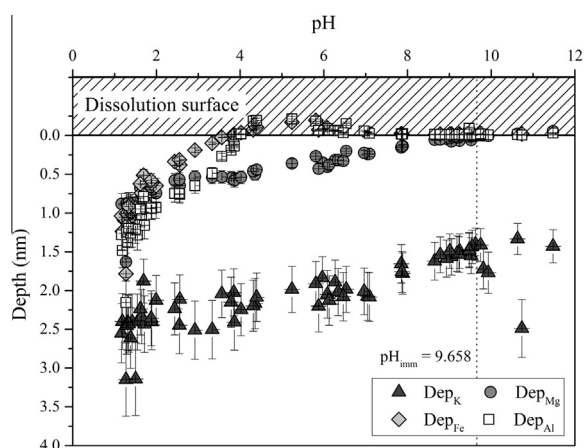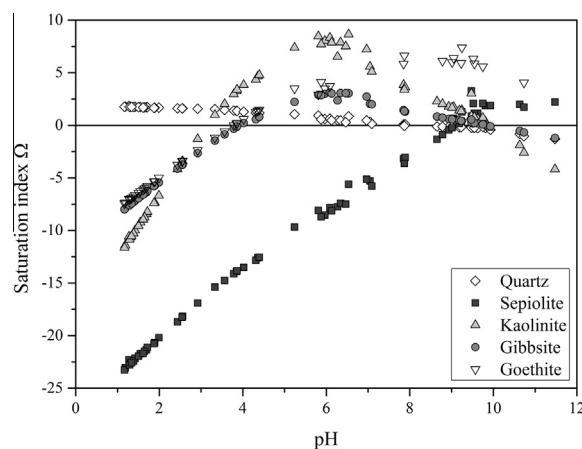

Fig. 8. Average bulk depth of depletion of exchanged metals from the dissolution surface as a function of pH. Depletion depth was calculated using Eq. (21). Error bars represent a 15% uncertainty in calculated depth and 0.002 pH uncertainty.

Fig. 9. A plot of saturation index of possible secondary phases in the titration experiments, as a function of pH. Phases include, Quartz (SiO_2), Sepiolite ($Mg_2Si_3O_7 \cdot 5OH \cdot 3H_2O$), Kaolinite ($Al_2Si_2O_5(OH)_4$), Gibbsite ($Al(OH)_3$) and Goethite (FeOOH). Saturation indicies were calculated using PHREEQC 3 (Parkhurst and Appelo, 2013).

between 36 and 240 times more reactive than the [0 0 1] basal. This phenomena suggests that depletion in the current study is likely far greater at the edges than at the basal surfaces. For example, if we assume that the edges comprise 5% of the total geometric surface area (e.g. Bonneville et al., 2011), and the edge:basal surface reactivity ratio is 71:1 (Hodson, 2006), we can calculate the relative depletion depths at the edge and basal surfaces. Note the assumption that edge surfaces are 5% of the total surface area may be a conservative estimate as this ratio increases with decreasing particle size. In the case of potassium, such a calculation presents depletion depths between 30 to 40 nm at the edges and up to 0.5 nm at the basal surface (Fig. S-2).

Taken together, these observations demonstrate that the biotite surface composition depends strongly on fluid pH. At basic conditions (pH > 8), biotite surfaces contain approximately stoichiometric proportions of Mg, Fe, Al and Si, but K seems to be completely depleted to a bulk average depth of 1.5 nm. At neutral conditions (pH 4 to 8), biotite surfaces are Fe and Al enriched and Mg and K poor, relative to Si. At acid conditions (pH < 4), the biotite surfaces contain partly detached silanol groups, >Si–OH0, following the removal of most of the univalent, divalent and trivalent metals. Additionally, at very low pH (<2) the bulk average metal depletion depth appears to increase dramatically (from 0.5 to 1.5 nm) with decreasing pH. Sheet silicates have been observed to preferentially dissolve parallel to the basal plane at low pH, promoting the removal of metals from deep within the mineral structure (Kaviratna and Pinnavaia, 1994; Turpault and Trotignon, 1994; Bickmore et al., 2001, 2003; Saldi et al., 2007). Saldi et al. (2007) presented photomicrographs displaying the fanning out of talc edges, exposing an increased reactive surface area. Such a mechanism could be responsible for the increased metal release from biotite we observe below pH 2 (Figs. 3, 4 and 8).

5.3. Biotite surface chemistry and charge

The results described above indicate that the surface composition of biotite differs significantly from the bulk, implying that the adsorption properties of biotite and phyllosilicates in general, likely differ significantly from predictions made solely from the bulk mineral compositions. For example, the pH_{ZPC} is commonly used to discuss surface charge. Although this has not been directly determined in this study, a number of approaches can be used to estimate pH_{ZPC}. For example, Parks (1967) suggested that the surface charge of multi oxide minerals can be estimated from the weighted sum of the constituent oxides, as used by Jara et al. (2005),

$$pH_{ZPC} = \sum_i pH_{IEP,i} X_i \qquad (22)$$

where X_i corresponds to the mole fraction of the ith oxide and $pH_{IEP,i}$ refers to the isoelectric point of the ith oxide. Using this approach, the pH_{ZPC} for biotite can be estimated to be 4.12 (Table 1). In contrast, the measured pH_{IEP} for biotite is 3.02, a value which is likely influenced by the observed metal depletion. Note the presence of calcite has little effect on the pH_{IEP} as it appears to have completely dissolved at pH < 4.

The biotite pH_{imm} value observed in this study (9.66), is vastly different from the measured pH_{IEP} (3.02) and calculated pH_{ZPC} (4.12). In a number of past studies, pH_{imm} has been assumed to equal pH_{ZNPC} (e.g. Amrhein and Suarez, 1988; Blum and Lasaga, 1991). The value of pH_{imm} is likely to not be influenced greatly by the presence of calcite as very little calcite dissolution occurred during the immersion period due to the high fluid pH. As discussed in Section 5.2, a pH_{imm} of 9.66 for biotite can be attributed to the partial charge conservation of K release during the immersion period. By subtracting from $[H^+]_{t=0}$ the net number of protons consumed by the sum of this exchange reaction, the dissolution of both biotite and calcite, and metal hydrolysis, we have calculated a pH_{ZNPC} for biotite of 7.50, comparable to reported pH_{ZPC} values for biotite 6.5 (Alonso, 2003 (as cited in Filby et al., 2008)) and 6–7 (Alonso et al., 2009), muscovite 6.6, and phlogopite 8 (Sverjensky, 1994), as summarised in Table 1.

However comparable our values for the various points of zero charge of biotite are to literature data, it is clear that the sole use of the ZPC, IEP, ZNPC or immersion pH to infer the surface charge of biotite at a given pH could provide an ambiguous picture of biotite surface chemistry. As previously proposed in Oelkers et al. (2009), accurate modelling the surfaces of complex multi-oxide silicates, e.g. phyllosilicates, requires the consideration of a changing surface composition as a function of the surrounding fluid chemistry.

5.4. Implications of biotite surface chemistry for dissolution kinetics as a function of aqueous solution composition

The dissolution mechanism of minerals has often been related to the chemical composition of the surface and the reactions occurring at the mineral–fluid interface (e.g. Furrer and Stumm, 1986; Brady and Walther, 1990). For the case of biotite, dissolution rates as a function of pH are similar to that of other aluminosilicates, in that they decrease with increasing pH in acidic conditions (i.e. up to pH 7) and increase thereafter with increasing pH (Lin and Clemency, 1981a,b; Acker and Bricker, 1992; Turpault and Trotignon, 1994; Kalinowski and Schweda, 1995; Malmström et al., 1996, 1997; Brandt et al., 2003; Balogh-Brunstad et al., 2008; Balland et al., 2010; Haward et al., 2011; Cappelli et al., 2013; Voinot et al., 2013). As the pH of minimum biotite dissolution rate (∼pH 7) differs from both pH_{IEP} (3.02) and pH_{imm} (9.66), it is clear that the biotite dissolution rates are not directly related to proton consumption at the surface. In contrast, the biotite surface reactivity appears to be dominated by non-charge conservative metal release, shown above to alter the surface composition of biotite as a function of pH. Such metal release involves the breaking of metal–oxygen bonds, both at the biotite surface and at a varying depth within the mineral, with a shift towards a relatively negatively charged biotite near-surface. The breaking of such bonds and the charge imbalance would weaken the biotite structure near the fluid interface, facilitating the mineral's eventual

dissolution. As such, it seems likely that such metal release reactions are critical in controlling, biotite dissolution rates, consistent with the dissolution pathways of a wide variety of other multi-oxide silicates (e.g. Gautier et al., 1994; Oelkers et al., 1994; Devidal et al., 1997; Gislason and Oelkers, 2003; Wolff-Boenisch et al., 2004; Carroll and Knauss, 2005; Saldi et al., 2007).

5.5. Implications for nutrient availability and bio-acquisition

As described above, a K depleted zone exists at all pH, extending to a bulk average depth of 2.5 nm, though this occurs primarily at the edges of the mineral grains (Fig. S-2). Indeed, the depletion depth of K at the edges of biotite grain varies from 25 up to 40 nm from a pH 1 to 11.5 while the K depletion on the basal planes barely exceeds a maximum of 0.5 nm at pH 1. This potassium depletion zone formed upon contact with water during the immersion period and this depth appears to be time independent for at least 60 min.

In a previous study (Bonneville et al., 2011), we have shown that the biotite basal plane can also be depleted in K and other elements such Al, Fe and Mg due to mycorrhizal alteration. Upon direct contact with the biotite surface, fungal hypha can mobilise K up to a depth of 20 nm for a pH range of 4.6–5.8 in the hypha near-environment. For the same pH range, the present study in an abiotic, water-saturated system shows that the basal plane K mobilisation is much more restricted, approximately 20 times less. This observation highlights the effectiveness of fungi to remove potassium from the biotite interlayer through a combination of the mechanical and chemical alteration pathways of the biotite in direct contact with hyphae. This alteration, or 'bio-fracking', comes in 4 forms: (i) forcing the crystallographic lattice of phyllosilicates (Bonneville et al., 2009), (ii) the creation of channels at the basal surface (Gazzè et al., 2012), (iii) the secretion of a biolayer up to 35 nm in thickness (Saccone et al., 2012) and, (iv) acidification of the hyphae near-environment at the biotite surface (Bonneville et al., 2011).

6. CONCLUSION

A combined approach of electrokinetic measurements, potentiometric batch titrations, and aqueous solution chemistry analyses have provided insight into the interaction of protons with the biotite surface. In brief, our results demonstrate the complex and variable nature of the biotite surface as a function aqueous fluid composition. Indeed, the ZPC, IEP, and immersion pH have vastly different values for biotite and therefore the sole use of zero points of charge provide an inaccurate depiction of biotite surface chemistry. Our study emphasises the need to consider the variable composition of the multi-oxide surface as a function of pH to accurately model the surface chemistry of those minerals and understand their chemical reactivity. The processes occurring at the biotite near-surface observed in this study help us to understand and interpret weathering reactions in microorganism dominated natural systems. The results of this study will be also be used further to aid the interpretation of biotite dissolution kinetics in our next study.

APPENDIX A. SUPPLEMENTARY DATA

Supplementary data associated with this article can be found, in the online version, at http://dx.doi.org/10.1016/j.gca.2013.12.002.

REFERENCES

Acker J. G. and Bricker O. P. (1992) The influence of pH on biotite dissolution and alteration kinetics at low temperature. *Geochim. Cosmochim. Acta* **56**, 3073–3092.

Adeyemi A. O. and Gadd G. M. (2005) Fungal degradation of calcium-, lead- and silicon-bearing minerals. *BioMetals* **18**, 269–281.

Alonso, U. (2003). Influencia de los coloides en el transporte de contaminantes en la interfaz campo cerano/campo lejano de un almacenamiento de residuos radioactivos de alta actividad. Ph.D. Thesis, Universidad Complutense de Madrid, Spain (in Spanish).

Alonso U., Missana T., Patelli A., Ceccato D., Albarran N., García-Gutiérrez M., Lopez-Torrubia T. and Rigato V. (2009) Quantification of Au nanoparticles retention on a heterogeneous rock surface. *Colloids Surf. A* **347**, 230–238.

Amrhein C. and Suarez D. L. (1988) The use of a surface complexation model to describe the kinetics of ligand-promoted dissolution of anorthite. *Geochim. Cosmochim. Acta* **52**, 2785–2793.

Balland C., Poszwa A., Leyval C. and Mustin C. (2010) Dissolution rates of phyllosilicates as a function of bacterial metabolic diversity. *Geochim. Cosmochim. Acta* **74**, 5478–5493.

Balogh-Brunstad Z., Keller C. K., Dickinson J. T., Stevens F., Li C. Y. and Bormann B. T. (2008) Biotite weathering and nutrient uptake by ectomycorrhizal fungus, *Sillus tomentosis*, in liquid-culture experiments. *Geochim. Cosmochim. Acta* **72**, 2601–2618.

Bickmore B. R., Bosbach D., Hochella M. F., Charlet L. and Rufe E. (2001) In situ atomic force microscopy study of hectorite and nontronite dissolution: implications for phyllosilicate edge

surface structures and dissolution mechanisms. *Am. Miner.* **86**, 411–423.

Bickmore B. R., Rosso K. M., Nagy K. L., Cygan R. T. and Tadanier C. J. (2003) *Ab initio* determination of edge surface structures for dioctahedral 2:1 phyllosilicates: implications for acid–base reactivity. *Clay Clay Miner.* **51**, 359–371.

Blum A. and Lasaga A. C. (1991) The role of surface speciation in the dissolution of albite. *Geochim. Cosmochim. Acta* **55**, 2193–2201.

Bonneville S., Smits M. M., Brown A., Harrington J., Leake J. R., Brydson R. and Benning L. G. (2009) Plant-driven fungal weathering: early stages of mineral alteration at the nanometer scale. *Geology* **37**, 615–618.

Bonneville S., Morgan D. J., Schmalenberger A., Bray A., Brown A., Banwart S. A. and Benning L. G. (2011) Tree-mycorrhiza symbiosis accelerate mineral weathering: evidences from nanometer-scale elemental fluxes at the hypha–mineral interface. *Geochim. Cosmochim. Acta* **75**, 6988–7005.

Bowser C. J. and Jones B. F. (2002) Mineralogic controls on the composition of natural waters dominated by silicate hydrolysis. *Am. J. Sci.* **302**, 582–662.

Brady P. V. and Walther J. V. (1990) Kinetics of quartz dissolution at low temperatures. *Chem. Geol.* **82**, 253–264.

Brandt F., Bosbach D., Krawczyk-Bärsch E., Arnold T. and Bernhard G. (2003) Chlorite dissolution in the acid pH-range: a combined microscopic and macroscopic approach. *Geochim. Cosmochim. Acta* **67**, 1451–1461.

Brigatti F. M., Frigieri P., Ghezzo C. and Poppi L. (2000) Crystal chemistry of Al-rich biotites coexisting with muscovites in peraluminous granites. *Am. Mineral.* **85**, 436–448.

Brown G. E. and Calas G. (2012) Mineral–aqueous solution interfaces and their impact on the environment. *Geochem. Perspect.* **1**, 483–742.

Brunauer S., Emmett P. H. and Teller E. (1938) Adsorption of gases in multimolecular layers. *J. Am. Chem. Soc.* **60**, 309–319.

Buss H. L., Lüttge A. and Brantley S. L. (2007) Etch pit formation on iron silicate surfaces during siderophore-promoted dissolution. *Chem. Geol.* **240**, 326–342.

Cappelli C., Van Driessche A. E. S., Cama J. and Huertas F. J. (2013) In situ observation of biotite dissolution at pH 1 using advanced optical microscopy. *Cryst. Growth Des.* **13**, 2880–2886.

Carroll S. A. and Knauss K. G. (2005) Dependence of labradorite dissolution kinetics on $CO_{2(aq)}$ and $Al_{(aq)}$ and temperature. *Chem. Geol.* **217**, 213–225.

Cases J. (1967) Les phenomenes physicochimiques a l'interface application au procede de la flottation. PhD thesis, Faculte des Sciences de L'Universite de Nancy.

Chaïrat C., Oelkers E. H., Schott J. and Lartigue J.-E. (2007) Fluorapatite surface composition in aqueous solution deduced from potentiometric, electrokinetic, and solubility measurements, and spectroscopic observations. *Geochim. Cosmochim. Acta* **71**, 5888–5900.

Davies C. W. (1962) *Ion Association*. Butterworths, London, 37–53.

Davis J. A. and Kent D. B. (1990) Surface complexation modelling in aqueous geochemistry. *Rev. Mineral. Geochem.* **23**, 117–260.

Devidal J.-L., Schott J. and Dandurand J.-L. (1997) An experimental study of kaolinite dissolution and precipitation kinetics as a function of chemical affinity and solution composition at 150 °C, 40 bars, and pH 2, 6.8 and 7.8. *Geochim. Cosmochim. Acta* **61**, 5165–5186.

Drever J. I. (1997) *The Geochemistry of Natural Waters*, 3rd ed. Prentice-Hall, New Jersey, 436.

Drever J. I. and Stillings L. L. (1997) The role of organic acids in mineral weathering. *Colloids Surf. A* **120**, 167–181.

Filby A., Plaschke M., Geckeis H. and Fanghänel Th. (2008) Interaction of latex colloids with mineral surfaces and Grimsel granodiorite. *J. Contam. Hydrol.* **102**, 273–284.

Furrer G. and Stumm W. (1986) The coordination chemistry of weathering: dissolution kinetics of Al_2O_3 and BeO. *Geochim. Cosmochim. Acta* **50**, 1847–1860.

Gadd G. M. (2007) Geomycology: biogeochemical transformations of rocks, minerals, metals and radionuclides by fungi, bioweathering and bioremediation. *Mycol. Res.* **111**, 3–49.

Gautier J.-M., Oelkers E. H. and Schott J. (1994) Experimental study of K-feldspar dissolution rates as a function of chemical affinity at 150 °C and pH 9. *Geochim. Cosmochim. Acta* **58**, 4549–4560.

Gazzè S. A., Saccone L., Ragnarsdottir K. V., Smits M. M., Duran A. L., Leake J. R., Banwart S. A. and McMaster T. J. (2012) Nanoscale channels on ectomycorrhizal-colonized chlorite: evidence for plant-driven fungal dissolution. *J. Geophys. Res.* **117**, G00N09.

Gislason S. R. and Oelkers E. H. (2003) The mechanism, rates and consequences of basaltic glass dissolution: II. An experimental study of the dissolution rates of basaltic glass as a function of pH at temperatures from 6 °C to 150 °C. *Geochim. Cosmochim. Acta* **67**, 3817–3832.

Haward S. J., Smitts M. M., Ragnarsdóttir K. V., Leake J. R., Banwart S. A. and McMaster T. J. (2011) In situ atomic force microscopy measurements of biotite basal plane reactivity in the presence of oxalic acid. *Geochim. Cosmochim. Acta* **75**, 6870–6881.

Hodson M. E. (2006) Does reactive surface area depend on grain size? Results from pH 3, 25 °C far-from-equilibrium flow-through experiments on anorthite and biotite. *Geochim. Cosmochim. Acta* **70**, 1655–1667.

Hunter R. J. (1989). .

IUPAC (2006) Compendium of Chemical Terminology, The Gold Book. <http://goldbook.iupac.org/>.

Jara A. A., Golberg S. and Mora M. L. (2005) Studies on the surface charge of amorphous aluminosilicates using surface complexation models. *J. Colloid Interface Sci.* **292**, 160–170.

James R. O. and Healy T. W. (1972) Adsorption of hydrolysable metal-ions at oxide water interface. 1. Co(II) adsorption on SiO_2 and TiO_2 as model systems. *J. Colloid Interface Sci.* **40**, 42–52.

Kaviratna H. and Pinnavaia T. J. (1994) Acid hydrolysis of octahedral Mg^{2+} sites in 2:1 layered silicates: an assessment of edge attack and gallery access mechanisms. *Clay Clay Miner.* **42**, 717–723.

Kalinowski B. E. and Schweda P. (1995) Kinetics of muscovite, phlogopite and biotite dissolution and alteration at pH 1–4, room temperature. *Geochim. Cosmochim. Acta* **60**, 367–385.

Kosmulski M. (2009) Compilation of PZC and IEP of sparingly soluble metal oxides and hydroxides from literature. *Adv. Colloid Interface Sci.* **152**, 14–25.

Leyval C. and Berthelin J. (1991) Weathering of a mica by roots and rhizospheric microorganisms of pine. *Soil Sci. Soc. Am. J.* **55**, 1009–1016.

Lian B., Chen Y., Zhu L. and Yang R. (2008) Effect of microbial weathering on carbonate rocks. *Earth Sci. Front.* **15**, 90–99.

Lin F.-C. and Clemency C. V. (1981a) Dissolution kinetics of phlogopite. I. Closed system. *Clay Clay Miner.* **29**, 101–106.

Lin F.-C. and Clemency C. V. (1981b) The kinetics of dissolution of muscovites at 25 °C and 1 atm CO_2 partial pressure. *Geochim. Cosmochim. Acta* **45**, 571–576.

Malmström M., Banwart S., Lewenhagen J., Duro L. and Bruno J. (1996) The dissolution of biotite and chlorite at 25 °C in the near-neutral pH region. *J. Contam. Hyrdol.* **21**, 201–213.

Malmström M. and Banwart S. (1997) Biotite dissolution at 25 °C: the pH dependence of dissolution rate and stoichiometry. *Geochim. Cosmochim. Acta* **61**, 2779–2799.

Momma K. and Izumi F. (2011) VESTA 3 for three-dimensional visualization of crystal, volumetric and morphology data. *J. Appl. Crystallogr.* **44**, 1272–1276.

Morel F. M. M. and Hering J. G. (1993) *Principles and Applications of Aquatic Chemistry*. Wiley, New York, Chapter 5, 297–318.

Oelkers E. H., Schott J. and Devidal J.-L. (1994) The effect of aluminium, pH, and chemical affinity on the rates of alumino-silicate dissolution reactions. *Geochim. Cosmochim. Acta* **58**, 661–669.

Oelkers E. H., Golubev S. V., Chaïrat C., Pokrovsky O. S. and Schott J. (2009) The surface chemistry of multi-oxide silicates. *Geochim. Cosmochim. Acta* **73**, 4617–4634.

Parkhurst D. L. and Appelo C. A. J. (2013) PHREEQC version 3 – a computer program for speciation, batch-reaction, one-dimensional transport, and inverse geochemical calculations. Available from: <http://wwwbrr.cr.usgs.gov/projects/GWC_coupled/phreeqc/>.

Parks G. A. (1965) Isoelectric points of solid oxides and aqueous hydroxo complex systems. *Chem. Rev.* **65**, 177–244.

Parks G. A. (1967) Aqueous surface chemistry of oxides and complex oxide minerals Stumm, W. (ed.). *Equilibrium Concepts in Natural Water Systems. Am. Chem. Soc. Adv. Chem.* **67**, 121–160.

Parks G. A. (1990) Surface energy and adsorption at mineral/water interfaces: an introduction. *Rev. Mineral.* **23**, 133–175.

Pokrovsky O. S., Schott J. and Thomas F. (1999) Dolomite surface speciation and reactivity in aquatic systems. *Geochim. Cosmochim. Acta* **63**, 3133–3143.

Pokrovsky O. S. and Schott J. (2000) Forsterite surface composition in aqueous solutions: a combined potentiometric, electrokinetic, and speciation approach. *Geochim. Cosmochim. Acta* **64**, 3299–3312.

Pokrovsky O. S. and Schott J. (2004) Experimental study of brucite dissolution and precipitation in aqueous solution: surface speciation and chemical affinity control. *Geochim. Cosmochim. Acta* **68**, 31–45.

Rath R. K. and Subramanian S. (1997) Studies on adsorption of guar gum onto biotite mica. *Miner. Eng.* **10**, 1405–1420.

Saccone L., Gazzè S. A., Duran A. L., Leake J. R., Banwart S. A., Ragnarsdóttir K. V., Smits M. M. and McMaster T. J. (2012) High resolution characterization of ectomycorrhizal fungal–mineral interactions in axenic microcosm experiments. *Biogeochemistry* **111**, 411–425.

Saldi G. D., Köhler S. J., Marty N. and Oelkers E. H. (2007) Dissolution rates of talc as a function of solution composition, pH and temperature. *Geochim. Cosmochim. Acta* **71**, 3446–3457.

Smits M. M., Bonneville S., Benning L. G., Banwart S. A. and Leake J. R. (2012) Plant-driven weathering of apatite – the role of an ectomycorrhizal fungus. *Geobiology* **10**, 445–456.

Sposito G. (1984) *The Surface Chemistry of Soils*. Oxford University Press, New York, 234p.

Sposito G. (1998) On points of zero charge. *Environ. Sci. Technol.* **32**, 2815–2819.

Sposito G. (2004) *The Surface Chemistry of Natural Particles*. Oxford University Press, New York, 242p.

Sverjensky D. A. (1994) Zero-point-of-charge prediction from crystal chemistry and solvation theory. *Geochim. Cosmochim. Acta* **58**, 3123–3129.

Sverjensky D. A. (2004) Prediction of surface charge on oxides in salt solutions: revisions for 1:1 (M^+L^-) electrolytes. *Geochim. Cosmochim. Acta* **69**, 225–257.

Turpault M. P. and Trotignon L. (1994) The dissolution of biotite single crystals in dilute HNO3 at 24 °C; evidence of an anisotropic corrosion process of micas in acidic solution. *Geochim. Cosmochim. Acta* **58**, 2761–2775.

Voinot A., Lemarchand D., Collignon C., Granet M., Chabaux F. and Turpault M.-P. (2013) Experimental dissolution vs. transformation of micas under acidic soil conditions: clues from boron isotopes. *Geochim. Cosmochim. Acta* **117**, 144–160.

Wallander H. and Wickman T. (1999) Biotite and microcline as potassium sources in ectomycorrhizal and non-mycorrhizal *Pinus sylvestris* seedlings. *Mycorrhiza* **9**, 25–32.

Webmineral.com. <http://webmineral.com/data/Biotite.shtml> (accessed April, 2013).

Wolff-Boenisch D., Gislason S. R. and Oelkers E. H. (2004) The effect of fluoride on the dissolution rates of natural glasses at pH 4 and 25 °C. *Geochim. Cosmochim. Acta* **68**, 4571–4582.

Associate editor: Jon Chorover